Structural characterization of the human membrane protein VDAC2 in lipid bilayers by MAS NMR

HHS Public Access

Author manuscript

J Biomol NMR. Author manuscript; available in PMC 2020 September 01.

Published in final edited form as:

J Biomol NMR. 2019 September ; 73(8-9): 451–460. doi:10.1007/s10858-019-00242-8.

Structural Characterization of the Human Membrane Protein VDAC2 in Lipid Bilayers by MAS NMR

Matthew T Eddy[1,2,*,†], **Tsyr-Yan Yu**[*,3,¥], **Gerhard Wagner**[3], **Robert G. Griffin**[1,2,‡]

[1]Department of Chemistry, Massachusetts Institute of Technology, Cambridge, MA 02139, USA

[2]Francis Bitter Magnet Laboratory, Massachusetts Institute of Technology, Cambridge, MA 02139, USA

[3]Department of Biological Chemistry and Molecular Pharmacology, Harvard Medical School, Boston, MA 02115, USA

Abstract

The second isoform of the human voltage dependent anion channel (VDAC2) is a mitochondrial porin that translocates calcium and other metabolites across the outer mitochondrial membrane. VDAC2 has been implicated in cardioprotection and plays a critical role in a unique apoptotic pathway in tumor cells. Despite its medical importance, there have been few biophysical studies of VDAC2 in large part due to the difficulty of obtaining homogeneous preparations of the protein for spectroscopic characterization. Here we present high resolution magic angle spinning (MAS) nuclear magnetic resonance (NMR) data obtained from homogeneous preparation of human VDAC2 in 2D crystalline lipid bilayers. The excellent resolution in the spectra permit several sequence-specific assignments of the signals for a large portion of the VDAC2 N-terminus and several other residues in two- and three-dimensional heteronuclear correlation experiments. The first 12 residues appear to be dynamic, are not visible in cross polarization experiments, and they are not sufficiently mobile on very fast timescales to be visible in ^{13}C INEPT experiments. A comparison of the NMR spectra of VDAC2 and VDAC1 obtained from highly similar preparations demonstrates that the spectral quality, line shapes and peak dispersion exhibited by the two proteins are nearly identical. This suggests an overall similar dynamic behavior and conformational homogeneity, which is in contrast to two earlier reports that suggested an inherent conformational heterogeneity of VDAC2 in membranes. The current data suggest that the sample preparation and spectroscopic methods are likely applicable to studying other human membrane porins, including human VDAC3, which has not yet been structurally characterized.

Introduction

Voltage-dependent anion channels (VDACs) are integral membrane proteins that transport metabolites across the outer mitochondrial surface. Humans express three VDAC isoforms (denoted hVDAC1, hVDAC2 and hVDAC3), which are predicted to have similar sizes and

‡Corresponding author: rgg@mit.edu.
†Present address: Departments of Chemistry, University of Florida, Gainesville, FL 32611, USA
¥Present address: Institute of Atomic and Molecular Sciences, Academia Sinica, Taipei, 10617, Taiwan
*Authors contributed equally

molecular weights[1]. Among these, hVDAC1 has been the most thoroughly studied in functional and biophysical assays[2–11]. In particular, structures of hVDAC1 and murine VDAC1 (mVDAC1) were solved by three independent groups, who each reported a 19-stranded β-barrel and an N-terminal alpha helix[12–14]. Despite the progress in understanding structure-function relationships of VDAC1, much less is known about the remaining two VDAC isoforms. For example, VDAC2 appears to play critical roles in human health and disease[15–19], but its underlying structural mechanisms for these roles are unclear. A crystal structure of zebrafish VDAC2 has been reported but that construct lacks the 11 amino acid extension of hVDAC2[20], and there is currently no published structure of human VDAC2. Thus, additional insights are needed into the structure-function relationship of human VDAC2, ideally in a native-like membrane environment.

Even though hVDAC1 and hVDAC2 share an overall 68% sequence homology, hVDAC2 exhibits unique cellular functions distinct from hVDAC1. Like VDAC1, VDAC2 also forms channels that transport ions and metabolites[10, 17, 19]. However, VDAC2 appears to have unique physiological roles distinct from VDAC1[21]. VDAC2 has been reported to play a role in apoptosis through its regulation of the pro-apoptotic protein BAK[22]. The small molecule erastin has been shown to selectively destroy cancer cells through formation of a complex with VDAC2 but not VDAC1[23]. Thus, VDAC2 may be an important target for the development of novel cancer treatments. It is possible that some of these functions are governed by the N-terminal tail that is 11 residues longer with a sequence MATHGQTCARP.

The aforementioned VDAC2 functional studies motivated application of magic angle spinning (MAS) nuclear magnetic resonance (NMR) spectroscopy to provide atomic-level structural details of VDAC2 in lipid bilayers. In earlier MAS NMR studies, homogeneous preparations of VDAC1 in lipid bilayers yielded spectra with excellent resolution, providing insights into the structure of VDAC1 in 2D lipid membranes[24–28]. To date, preparations of VDAC2 in lipid bilayers for MAS NMR have not yielded spectra of similar quality to VDAC1, prohibiting identification of individual resonances and their *de novo* assignment[29, 30]. These observations suggested that there are present inherent differences in the conformational homogeneity of VDAC1 and VDAC2. In contrast, we report here advances in the preparation of VDAC2 reconstituted into lipid bilayers that yield MAS spectra of comparable quality to those published earlier for VDAC1. The data permit identification of many residues in the functionally-important N-terminus and allow us to compare some features of the structures of VDAC1 and VDAC2 spectroscopically.

Results

Sample characterization and two-dimensional homonuclear correlation experiments

To obtain samples for MAS NMR studies of VDAC2 in lipid bilayers, we followed our previously reported method for preparation of VDAC1 in 2D lipid crystals[26]. From this protocol, we obtained 2D crystals of VDAC2 reconstituted into DMPC lipid bilayers. Figure 1A shows a representative negative stain electron micrograph of VDAC2/DMPC 2D crystals. The average particle size of the 2D crystals was approximately 1–3 μm in diameter, and the overall appearance was similar to VDAC1 DMPC crystals[26].

We initially characterized VDAC2 samples with solid state NMR by recording one-dimensional ^{13}C Bloch decay, ^{13}C cross polarization (CP)[31], and ^{13}C INEPT[32] spectra to qualitatively probe protein dynamics. In earlier MAS NMR studies, comparison of these experiments was used to reveal mobile regions of membrane-embedded proteins such as loops or extended termini that undergo very fast (ns) time scale motions[33–37]. Figure 1B–D compare these three experiments in representative one-dimensional spectra recorded with uniformly ^{13}C and ^{15}N-labeled VDAC2 in DMPC. Taking into account the different number of scans, the integrated intensity of the ^{13}C CP spectrum is approximately a factor of 1.5 to 2 times more intense than the Bloch decay spectrum. In contrast, the ^{13}C INEPT spectrum shows almost no signals, indicating that there is little to no motion on very fast timescales.

Two-dimensional ^{13}C–^{13}C NMR correlation experiments showed that our preparations of VDAC2 in lipid bilayers yielded homogeneous samples. Figure 2 shows the aliphatic region of a representative ^{13}C–^{13}C 2D correlation experiment recorded with short RFDR[38, 39] mixing to obtain predominantly one-bond correlations. The spectrum is highly dispersed with many well resolved signals, consistent with properly folded VDAC2 in DMPC. ^{13}C line widths in the spectrum were remarkably narrow, typically <0.5 ppm for resolved resonances. Signal intensities were overall fairly uniform, though the most intense signals were identified in 3D correlation experiments as arising from portions of the N-terminus. These narrow signals permitted resonance assignments in 2D and 3D experiments as well as direct comparison with spectra of uniformly labeled VDAC1 (see Discussion). Resonance assignments were obtained with 3D ^{15}N-^{13}C-^{13}C experiments[40–42]. In this case we employed a ZF-TEDOR-RFDR correlation experiment[43–45] using as starting points assignments obtained for several residues from 2D ^{13}C-^{13}C and ^{15}N-^{13}C correlation experiments.

Figure 2B shows an expansion of the aliphatic region where mostly Pro Cβ−Cδ and Ala Cα−Cβ correlations are observed. Out of a total of seven prolines in the VDAC2 amino acid sequence, we observed strong signals for four Pro Cβ−Cδ and two weaker signals that were partially overlapped by the more intense resonances. We observed five signals in the Ala Cα−Cβ region with Cβ chemical shifts between 18 and 22 ppm, which is a characteristic region for signals from Ala residues in alpha helices or loops. Two of these signals, Ala24 and Ala25, were completely overlapped in the 2D ^{13}C–^{13}C correlation spectrum but were resolved in 3D heteronuclear correlation spectra. The remaining Ala Cβ signals were shifted downfield and highly overlapped in the 2D spectra with chemical shifts that were consistent with β–barrel secondary structure. Figure 2C shows predominantly one-bond Cα−Cβ correlations for various residues. In Figure 2D, resolved ^{13}C–^{13}C signals from Thr and Ser amino acid types are shown. For Thr one-bond correlations, three resolved signals are observed with simultaneous upfield-shifted Cβ downfield-shifted Cα chemical shifts, roughly characteristic of α-helical secondary structure; whereas for Ser one-bond correlations, five to six signals were observed with chemical shifts characteristic of alpha helical secondary structure. The remaining Thr and Ser signal intensities were observed to be much more highly overlapped in regions of the spectra that typically correlate with signals from β–strand secondary structure.

Two and three-dimensional heteronuclear correlation experiments and assignments of VDAC2 in lipid bilayers

To confirm the identity of spin systems from the 2D ^{13}C–^{13}C correlation data, we recorded 2D heteronuclear ^{15}N–^{13}C correlation spectra. Figure 3 shows a representative 2D ^{15}N–^{13}C correlation spectrum measured with ZF-TEDOR mixing[44] optimized for one-bond transfers. Numerous resolved signals could be observed in both the upfield N–C' and downfield N–Cα spectral regions with typical ^{15}N linewidths of 0.5 ppm or less and uniform signal intensities for many resonances. Four unique proline Cα−Cδ spin systems could be readily identified from their unique ^{15}N chemical shifts between 134 and 144 ppm, and the C' resonance from residues preceding prolines were also identified. By analyzing the resolved proline signals in the TEDOR spectrum in combination with the 2D ^{13}C–^{13}C RFDR correlation spectrum, and by observing the closely similar positions of signals to corresponding Pro 4 and Pro 5 in VDAC1, chemical shifts were tentatively assigned for residues Ile14-Pro15-Pro16. These assignments were later confirmed in 3D ^{15}N-^{13}C-^{13}C correlation experiments because these are the only two consecutive prolines in the VDAC2 amino acid sequence. Additionally, assignments for Pro240 and Pro264 and the directly preceding residues were made by comparison of 2D ^{13}C–^{13}C RFDR and ^{15}N–^{13}C TEDOR spectra between VDAC2 and VDAC1 in 2D lipid crystals[24, 26] and by the fact that the two sequences share a large degree of similarity (see Figure S1). The corresponding residues in VDAC1 are Pro229 and Pro253. Signals from these Pro residues are identical in ^{13}C–^{13}C RFDR correlation spectra of VDAC2 and VDAC1 (see Figure 5), and the two amino acid sequences are also nearly identical in these regions.

The 3-dimensional ^{15}N-^{13}C-^{13}C correlation experiment was recorded using a ZF-TEDOR-RFDR pulse sequence that obtains both NCOCX and NCACX connectivity data in a single spectrum. As it has been noted in the literature[43, 45], this experiment also provides improved sensitivity for Pro residues, because the initial polarization step utilizes H–C cross polarization rather than H–N cross polarization. In this experiment, one-bond ^{15}N-^{13}C TEDOR mixing was followed by a relatively short RFDR mixing period to obtain N(i)–Cα(i)–Cβ(i) and N(i)–C'(i-1)-Cα/Cβ(i-1) correlations. The indirect dwell in the ^{15}N dimension was synchronized to twice the rotor period to fold the ^{15}N side bands onto the centerband.

Figure 4 shows representative strip plots from the 3D zf-TEDOR-RFDR spectrum, where individual panels were selected from the NCACX and NCOCX regions of the spectrum to illustrate sequential assignments for residues Pro15 to Ala19. By analyzing the 3-dimensional and 2-dimensional data sets together, backbone and side chain resonances for residues Cys13 through Phe29 were assigned with the exception of G22. The chemical shifts assigned to these residues are listed in Table 1. While Ala24 and Ala25 Cα–Cβ correlations were overlapped in 2D ^{13}C–^{13}C RFDR experiments, their ^{15}N resonances were well separated enabling unambiguous assignments. In addition, more unique spin systems could be identified in the 3D data sets, including resolved Ala Cα–Cβ signals with chemical shifts consistent with beta strand secondary structure, but unambiguous sequential assignments could not be directly confirmed.

Discussion

The MAS NMR data presented here are intriguing in the context of earlier NMR studies of VDAC2 in lipid bilayers. Gattin, et al[29] reconstituted human VDAC2 into DMPC lipids and recorded ^{13}C–^{13}C correlation experiments. In their study, comparisons of NMR spectra of VDAC2 and VDAC1 revealed significantly broader NMR lines and relatively few resolved signals for VDAC2. This comparison motivated the authors to conclude that VDAC2 preparations in lipid bilayers were more heterogeneous than corresponding preparations of VDAC1 in lipids. A similar observation was reported in an earlier study by Bauer, et al.[30], where preparations of human VDAC2 reconstituted into lipid bilayers yielded solid state NMR spectra that were too broad to observe individually resolved signals.

A critical step to obtain homogeneous preparations of VDAC2 in lipid bilayers was the proper refolding of VDAC2 in buffer containing LDAO detergent and the isolation of monodispersed and folded protein prior to reconstitution in lipid bilayers. VDAC2 refolding was found to be particularly sensitive to the presence of minor impurities found in commercially available LDAO. The highest levels of refolded VDAC2 were obtained by using LDAO that was further purified by recrystallization (FBReagents). Properly folded VDAC2 was then isolated by consecutive ion exchange and size exclusion chromatography of the refolded product. Reconstitution of folded VDAC2 into lipid bilayers was carried out identically to protocols used for VDAC1[26].

For our preparation of hVDAC2 in DMPC lipid bilayers, the MAS spectra are remarkably well resolved and of similar quality to our earlier studies of human VDAC1 in DMPC lipid bilayers[25, 26]. Figure 5 shows a comparison of 2D ^{13}C-^{13}C RFDR correlation spectra of uniformly ^{15}N,^{13}C-labeled VDAC2 and VDAC1 where both proteins were reconstituted into DMPC lipid bilayers. The number of signals and line widths of resolved signals is similar in the two spectra, indicating that the overall homogeneity of the two proteins is highly similar in 2D crystals of lipid bilayer. Thus, these data stand in contrast to earlier studies and suggest that observed spectral heterogeneity reported previously is more likely due to details of the sample preparation rather than a heterogeneous distribution of conformational states that is inherent to VDAC2 in lipid bilayers.

The high quality of our solid state NMR data yields initial insights into the VDAC2 secondary structure. Overall, analysis of ^{13}C chemical shifts for VDAC2 signals indicate a greater extent of β-barrel represented in the secondary structure. The range of predicted chemical shifts from a SHIFTX2 calculation using the zebrafish VDAC2 crystal structure (PDB 4BUM) appear qualitatively similar to the range of experimentally observed human VDAC2 signals (Figure S3). In our preparations of human VDAC2, signals for residues Pro15 through Phe29 were strong and well resolved, while signals for Cys13 and Ile14 were significantly weaker. Signals for residues Met1 through Met12 could not be assigned in any of the 2D or 3D correlation spectra. The missing resonances include Pro11, which would have been readily observed in either ^{13}C–^{13}C or ^{15}N–^{13}C correlation experiments. Weaker spectral features were observed in the Pro Cβ–Cδ region of the RFDR spectrum but these signals were significantly weaker than the 4 assigned Pro signals and could not be confirmed in heteronuclear correlation experiments. Thus, we hypothesize that signals for Pro11 and

possibly at least some residues preceding it are substantially broadened from conformational dynamics in the dipolar-based recoupling experiments, possibly due to interference with ^{1}H decoupling or cross polarization[46,47]. The absence of a clear INEPT signal (Figure 1) indicates that motion associated with the first 12 residues is not in the fast limit. Analysis of secondary chemical shifts[48] for assigned VDAC2 residues 13 to 29 (Figure 5D) revealed a propensity for alpha helical secondary structure for residues 18–19 and 23–29 with an extended conformation for residues 13 to 17.

The present characterization of human VDAC2 in lipid bilayers and initial assignments provide a promising point of departure for future high resolution studies of VDAC2. As noted above, there currently exist no published structures of human VDAC2. A more complete study of these VDAC2 samples is in progress and will include additional ^{13}C-^{13}C and ^{13}C-^{15}N, as well as ^{1}H detected, MAS spectra which will be required for a complete structural determination. Functional studies of the VDAC family will likely require low temperatures to trap intermediates and determine drug binding sites, an approach that has been successfully applied to bacteriorhodopsin[49, 50] and $M2_{18–60}$ from influenza-A[51, 52]. Furthermore, no structural information yet exists for the third isoform of human VDAC. Based on the current results, it appears that high resolution studies of the structure and function VDAC3 in lipid bilayers by solid state NMR will be feasible.

Experimental Section

Materials

1,2-Dymyristoyl-*sn*-glycero-3-phosphocholine (DMPC) was purchased from Avanti Polar Lipids (Alabaster, AL). Octylpolyoxyethylene (octyl-POE) was purchased from Bachem (King of Prussia, PA). All other non-isotopically labeled reagents were purchased from Fisher. Isotopically labeled reagents used for VDAC2 expression were obtained from Cambridge Isotope Labs (Andover, MA).

Recombinant expression, refolding, and purification of human VDAC2

Human VDAC2 was expressed in Rosetta 2(DE3) cells by induction with 1 mM IPTG at 37°C for 12 hours. Purification and refolding of isolated VDAC2 was done according to previously published protocols[53]. Briefly, inclusion bodies containing VDAC2 were dissolved in buffer containing 8M urea, and VDAC2 was isolated under denaturing conditions by nickel affinity chromatography. Purified VDAC2 was precipitated in buffer (50 mM Tris–HCl, 50 mM NaCl, 1 mM EDTA, 5 mM DTT, pH 7.0), dissolved in buffer containing 6M guanidine hydrochloride, and refolded in buffer containing 1.5% LDAO. The LDAO was purchased from Anatrace and further purified prior to refolding (FB Reagents). Properly refolded product was isolated by consecutive ion exchange and size exclusion chromatography steps. The improved quality of MAS spectra is likely due to a more homogenous population of refolded VDAC2 in LDAO detergent micelles. This was achieved by using LDAO that had been further purified by FB Reagents, and the use of both ion exchange and size exclusion chromatography steps following refolding to remove impurities.

Preparation of hVDAC2/DMPC 2D crystals

Protocols for preparation of hVDAC2/DMPC 2D crystals followed earlier preparation of hVDAC1/DMPC 2D crystals in Eddy et al.[26], which were modified from the protocol originally described by Dolder et al.[54] Briefly, purified VDAC2 in LDAO was exchanged into buffer containing octyl-POE. This was followed by addition of DMPC lipids and dialysis to remove the detergent.

Mass spectra of VDAC2

We determined the molecular weight of the VDAC2 construct employed in the current study with mass spectrometry to be 32.4 kDa. This molecular weight is consistent with the predicted molecular weight of VDAC2 with an intact N-terminus. Thus, we can conclude that all N-terminal residues are expressed and remain covalently attached to the protein. We have included the full VDAC2 sequence and the mass spectrometry data in a new supporting information section.

NMR spectroscopy

All spectra were recorded with a single ^{13}C,^{15}N labeled sample of VDAC2/DMPC 2D crystals, containing approximately 16 mg of VDAC2 and 8 mg of DMPC packed into a Bruker 3.2 mm MAS rotor. 1D ^{13}C spectra were acquired using dipolar based cross polarization (CP) and INEPT[32] at $\omega_{0H}/2\pi$=900 MHz, $\omega_r/2\pi$=20.0 kHz MAS frequency and T=290 K. 2D homonuclear ^{13}C–^{13}C correlation spectra were acquired with RFDR mixing at $\omega_r/2\pi$=20.0 kHz MAS and $\omega_{0H}/2\pi$=900 MHz on an Avance II spectrometer equipped with a 3.2 mm E-Free MA probe (Bruker Biospin, Billerica, MA). 2D ^{15}N–^{13}C correlation spectra were acquired using ZF-TEDOR[55, 56].

3D ^{15}N–^{13}C–^{13}C correlation spectra were acquired with a ZF-TEDOR-RFDR pulse sequence implementing ^{15}N–^{13}C TEDOR mixing followed by ^{13}C–^{13}C RFDR mixing, as previously described[43, 45].

Supplementary Material

Refer to Web version on PubMed Central for supplementary material.

Acknowledgements

This research was supported by NIH Grants EB001960 and EB002026. MTE acknowledges support from an American Cancer Society postdoctoral research fellowship. The authors thanks Mr. Frans Ricardo for MALDI mass spectrometry characterization of VDAC2.

References

[1]. Raghavan A, Sheiko T, Graham BH, and Craigen WJ (2012) Voltage-dependant anion channels: Novel insights into isoform function through genetic models, BBA - Biomembranes 1818, 1477–1485. [PubMed: 22051019]

[2]. Colombini M (2016) The VDAC channel: Molecular basis for selectivity, BBA - Molecular Cell Research, 1–19.

[3]. Colombini M (2012) VDAC structure, selectivity, and dynamics, BBA - Biomembranes 1818, 1457–1465. [PubMed: 22240010]

[4]. Colombini M (2004) VDAC: the channel at the interface between mitochondria and the cytosol., Molecular and cellular biochemistry 256–257, 107–115.

[5]. Rostovtseva T, and Colombini M (1997) VDAC channels mediate and gate the flow of ATP: implications for the regulation of mitochondrial function, Biophysical journal 72, 1954–1962. [PubMed: 9129800]

[6]. Rostovtseva T, and Colombini M (1996) ATP flux is controlled by a voltage-gated channel from the mitochondrial outer membrane., The Journal of biological chemistry 271, 28006–28008. [PubMed: 8910409]

[7]. Rostovtseva TK, and Bezrukov SM (1998) ATP Transport Through a Single Mitochondrial Channel, VDAC, Studied by Current Fluctuation Analysis, Biophysj 74, 2365–2373.

[8]. Colombini M (1979) A candidate for the permeability pathway of the outer mitochondrial membrane., Nature 279, 643–645. [PubMed: 450112]

[9]. Blachly-Dyson E, Peng S, Colombini M, and Forte M (1990) Selectivity changes in site-directed mutants of the VDAC ion channel: structural implications., Science 247, 1233–1236. [PubMed: 1690454]

[10]. Blachly-Dyson E, Zambronicz EB, Yu WH, Adams V, McCabe ER, Adelman J, Colombini M, and Forte M (1993) Cloning and functional expression in yeast of two human isoforms of the outer mitochondrial membrane channel, the voltage-dependent anion channel., Journal of Biological Chemistry 268, 1835–1841. [PubMed: 8420959]

[11]. Zizi M, Forte M, Blachly-Dyson E, and Colombini M (1994) NADH regulates the gating of VDAC, the mitochondrial outer membrane channel., Journal of Biological Chemistry 269, 1614–1616. [PubMed: 7507479]

[12]. Ujwal R, Cascio D, Colletier J-P, Faham S, Zhang J, Toro L, Ping P, and Abramson J (2008) The crystal structure of mouse VDAC1 at 2.3 A resolution reveals mechanistic insights into metabolite gating., Proceedings of the National Academy of Sciences USA 105, 17742–17747.

[13]. Bayrhuber M, Meins T, Habeck M, Becker S, Giller K, Villinger S, Vonrhein C, Griesinger C, Zweckstetter M, and Zeth K (2008) Structure of the human voltage-dependent anion channel., Proceedings of the National Academy of Sciences USA 105, 15370–15375.

[14]. Hiller S, Garces RG, Malia TJ, Orekhov VY, Colombini M, and Wagner G (2008) Solution structure of the integral human membrane protein VDAC-1 in detergent micelles., Science 321, 1206–1210. [PubMed: 18755977]

[15]. Lauterwasser J, Todt F, Zerbes RM, Nguyen TN, Craigen W, Lazarou M, van der Laan M, and Edlich F (2016) The porin VDAC2 is the mitochondrial platform for Bax retrotranslocation., Nature 6, 32994.

[16]. Liu B, Wang Z, Zhang W, and Wang X (2009) Expression and localization of voltage-dependent anion channels (VDAC) in human spermatozoa, Biochemical and Biophysical Research Communications 378, 366–370. [PubMed: 19013129]

[17]. Naghdi S, and Hajnóczky G (2016) VDAC2-specific cellular functions and the underlying structure, BBA - Molecular Cell Research 1863, 2503–2514. [PubMed: 27116927]

[18]. Yoo BC, Fountoulakis M, Cairns N, and Lubec G (2001) Changes of voltage-dependent anion-selective channel proteins VDAC1 and VDAC2 brain levels in patients with Alzheimer's disease and Down Syndrome, ELECTROPHORESIS 22, 172–179. [PubMed: 11197169]

[19]. Maurya SR, and Mahalakshmi R (2016) Mitochondrial VDAC2 and cell homeostasis: highlighting hidden structural features and unique functionalities, Biological Reviews 279, 25364–25316.

[20]. Schredelseker J, Paz A, Lopez CJ, Altenbach C, Leung CS, Drexler MK, Chen JN, Hubbell WL, and Abramson J (2014) High Resolution Structure and Double Electron-Electron Resonance of the Zebrafish Voltage-dependent Anion Channel 2 Reveal an Oligomeric Population, The Journal of biological chemistry 289, 12566–12577. [PubMed: 24627492]

[21]. Menzel VA, Cassará MC, Benz R, De Pinto V, Messina A, Cunsolo V, Saletti R, Hinsch KD, and Hinsch E (2009) Molecular and functional characterization of VDAC2 purified from mammal spermatozoa, Bioscience Reports 29, 351–362. [PubMed: 18976238]

[22]. Cheng EHY, Sheiko TV, Fisher JK, Craigen WJ, and Korsmeyer SJ (2003) VDAC2 inhibits BAK activation and mitochondrial apoptosis., Science 301, 513–517. [PubMed: 12881569]

[23]. Yagoda N, von Rechenberg M, Zaganjor E, Bauer AJ, Yang WS, Fridman DJ, Wolpaw AJ, Smukste I, Peltier JM, Boniface JJ, Smith R, Lessnick SL, Sahasrabudhe S, and Stockwell BR (2007) RAS–RAF–MEK-dependent oxidative cell death involving voltage-dependent anion channels, Nature 447, 865–869.

[24]. Eddy MT, Su Y, Silvers R, Andreas L, Clark L, Wagner G, Pintacuda G, Emsley L, and Griffin RG (2015) Lipid bilayer-bound conformation of an integral membrane beta barrel protein by multidimensional MAS NMR, Journal of Biomolecular NMR 61, 299–310. [PubMed: 25634301]

[25]. Eddy MT, Andreas L, Teijido O, Su Y, Clark L, Noskov SY, Wagner G, Rostovtseva TK, and Griffin RG (2015) Magic angle spinning nuclear magnetic resonance characterization of voltage-dependent anion channel gating in two-dimensional lipid crystalline bilayers., Biochemistry 54, 994–1005. [PubMed: 25545271]

[26]. Eddy MT, Ong T-C, Clark L, Teijido O, van der Wel PCA, Garces R, Wagner G, Rostovtseva TK, and Griffin RG (2012) Lipid dynamics and protein-lipid interactions in 2D crystals formed with the β-barrel integral membrane protein VDAC1., Journal of the American Chemical Society 134, 6375–6387. [PubMed: 22435461]

[27]. Schneider R, Etzkorn M, Giller K, Daebel V, Eisfeld J, Zweckstetter M, Griesinger C, Becker S, and Lange A (2010) The native conformation of the human VDAC1 N terminus., Angewandte Chemie. International Ed. In English 49, 1882–1885. [PubMed: 20140924]

[28]. Zachariae U, Schneider R, Briones R, Gattin Z, Demers J-P, Giller K, Maier E, Zweckstetter M, Griesinger C, Becker S, Benz R, de Groot BL, and Lange A (2012) β-Barrel mobility underlies closure of the voltage-dependent anion channel., Structure 20, 1540–1549. [PubMed: 22841291]

[29]. Gattin Z, Schneider R, Laukat Y, Giller K, Maier E, Zweckstetter M, Griesinger C, Benz R, Becker S, and Lange A (2015) Solid-state NMR, electrophysiology and molecular dynamics characterization of human VDAC2., Journal of Biomolecular NMR 61, 311–320. [PubMed: 25399320]

[30]. Bauer AJ, Gieschler S, Lemberg KM, McDermott AE, and Stockwell BR (2011) Functional Model of Metabolite Gating by Human Voltage-Dependent Anion Channel 2, Biochemistry 50, 3408–3410. [PubMed: 21425834]

[31]. Pines A, Gibby MG, and Waugh JS (1973) Proton-enhanced NMR of dilute spins in solids, The Journal of Chemical Physics 59, 569–590.

[32]. Morris GA, and Freeman R (1979) Enhancement of nuclear magnetic resonance signals by polarization transfer, Journal of the American Chemical Society 101, 760–762.

[33]. Etzkorn M, Martell S, Andronesi OC, Seidel K, Engelhard M, and Baldus M (2007) Secondary Structure, Dynamics, and Topology of a Seven-Helix Receptor in Native Membranes, Studied by Solid-State NMR Spectroscopy, Angewandte Chemie International Edition 46, 459–462. [PubMed: 17001715]

[34]. Andronesi OC, Becker S, Seidel K, Heise H, Young HS, and Baldus M (2005) Determination of Membrane Protein Structure and Dynamics by Magic-Angle-Spinning Solid-State NMR Spectroscopy †, Journal of the American Chemical Society 127, 12965–12974. [PubMed: 16159291]

[35]. Ward ME, Brown LS, and Ladizhansky V (2015) Advanced solid-state NMR techniques for characterization of membrane protein structure and dynamics: Application to Anabaena Sensory Rhodopsin, Journal of Magnetic Resonance 253, 119–128. [PubMed: 25637099]

[36]. Stehle J, Scholz F, Löhr F, Reckel S, Roos C, Blum M, Braun M, Glaubitz C, Dötsch V, Wachtveitl J, and Schwalbe H (2012) Characterization of the ground state dynamics of proteorhodopsin by NMR and optical spectroscopies, Journal of Biomolecular NMR 54, 401–413. [PubMed: 23160927]

[37]. Zhong L, Bamm VV, Ahmed MAM, Harauz G, and Ladizhansky V (2007) Solid-state NMR spectroscopy of 18.5 kDa myelin basic protein reconstituted with lipid vesicles: Spectroscopic characterisation and spectral assignments of solvent-exposed protein fragments, Biochimica et Biophysica Acta (BBA) - Biomembranes 1768, 3193–3205. [PubMed: 17920035]

[38]. Bennett AE, Rienstra CM, Griffiths JM, Zhen W, Lansbury PT Jr., and Griffin RG (1998) Homonuclear radio frequency-driven recoupling in rotating solids, The Journal of Chemical Physics 108, 9463–9479.

[39]. Bennett AE, Griffin RG, Ok JH, and Vega S (1992) Chemical shift correlation spectroscopy in rotating solids: Radio frequency-driven dipolar recoupling and longitudinal exchange, The Journal of Chemical Physics 96, 8624–8627.

[40]. Jaroniec CP, Tounge BA, Rienstra CM, Herzfeld J, and Griffin RG (1999) Measurement of C-13-N-15 distances in uniformly C-13 labeled biomolecules: J-decoupled REDOR, Journal of the American Chemical Society 121, 10237–10238.

[41]. Rienstra CM, Hohwy M, Hong M, and Griffin RG (2000) 2D and 3D N-15-C-13-C-13 NMR chemical shift correlation spectroscopy of solids: Assignment of MAS spectra of peptides, Journal of the American Chemical Society 122, 10979–10990.

[42]. Sun BQ, Rienstra CM, Costa PR, Williamson JR, and Griffin RG (1997) 3D 15N-13C-13C Chemical Shift Correlation Spectroscopy in Rotating Solids, 10 9 1997 119, 8540–8546.

[43]. Daviso E, Eddy MT, Andreas LB, Griffin RG, and Herzfeld J (2013) Efficient resonance assignment of proteins in MAS NMR by simultaneous intra- and inter-residue 3D correlation spectroscopy, Journal of Biomolecular NMR 55, 257–265. [PubMed: 23334347]

[44]. Jaroniec CP, Filip C, and Griffin RG (2002) 3D TEDOR NMR experiments for the simultaneous measurement of multiple carbon-nitrogen distances in uniformly C-13, N-15-labeled solids, J Am Chem Soc 124, 10728–10742. [PubMed: 12207528]

[45]. Andreas LB, Eddy MT, Chou JJ, and Griffin RG (2012) Magic-Angle-Spinning NMR of the Drug Resistant S31N M2 Proton Transporter from Influenza A, Journal of the American Chemical Society 134, 7215–7218. [PubMed: 22480220]

[46]. Maus DC, Copié V, Sun B, Griffiths JM, Griffin RG, Luo S, Schrock RR, Liu AH, Seidel SW, Davis WM, and Grohmann A (1996) A Solid-State NMR Study of Tungsten Methyl Group Dynamics in [W(η 5-C 5Me 5)Me 4][PF 6], Journal of the American Chemical Society 118, 5665–5671.

[47]. Long JR, Sun BQ, Bowen A, and Griffin RG (1994) Molecular Dynamics and Magic Angle Spinning NMR, Journal of the American Chemical Society 116, 11950–11956.

[48]. Luca S, Filippov DV, van Boom JH, Oschkinat H, de Groot HJ, and Baldus M (2001) Secondary chemical shifts in immobilized peptides and proteins: a qualitative basis for structure refinement under magic angle spinning., Journal of Biomolecular NMR 20, 325–331. [PubMed: 11563556]

[49]. Bajaj VS, Mak-Jurkauskas ML, Belenky M, Herzfeld J, and Griffin RG (2009) Functional and shunt states of bacteriorhodopsin resolved by 250-GHz dynamic nuclear polarization-enhanced solid-state NMR Proc. Nat'l. Acad. Sci 106, 9244–9249. [PubMed: 19474298]

[50]. Ni QZ, Can TV, Daviso E, Belenky M, Griffin RG, and Herzfeld J (2018) Primary Transfer Step in the Light-Driven Ion Pump Bacteriorhodopsin: An Irreversible U-Turn Revealed by Dynamic Nuclear Polarization-Enhanced Magic Angle Spinning NMR, Journal of the American Chemical Society 140, 4085–4091. [PubMed: 29489362]

[51]. Andreas LB, Barnes AB, Corzilius B, Chou JJ, Miller EA, Caporini M, Rosay M, and Griffin RG (2013) Dynamic Nuclear Polarization Study of Inhibitor Binding to the M2 Proton Transporter from Influenza A, Biochemistry 52, 2774–2782. [PubMed: 23480101]

[52]. Andreas LB, Reese M, Eddy MT, Gelev V, Ni QZ, Miller EA, Emsley L, Pintacuda G, Chou JJ, and Griffin RG (2015) Structure and Function of the Influenza A M218–60 Dimer of Dimers, Jour Amer Chem Soc 137, 14877–14866. [PubMed: 26218479]

[53]. Yu T-Y, Raschle T, Hiller S, and Wagner G (2012) Solution NMR spectroscopic characterization of human VDAC-2 in detergent micelles and lipid bilayer nanodiscs, BBA - Biomembranes 1818, 1562–1569. [PubMed: 22119777]

[54]. Dolder M, Zeth K, Tittmann P, Gross H, Welte W, and Wallimann T (1999) Crystallization of the human, mitochondrial voltage-dependent anion-selective channel in the presence of phospholipids., Journal of structural biology 127, 64–71. [PubMed: 10479618]

[55]. Hing AW, Vega S, and Schaefer J (1993) Measurement of heteronuclear dipolar coupling by transferred-echo double-resonance NMR, Journal of Magnetic Resonance, Series A 103, 151–162.

[56]. Jaroniec CP, Filip C, and Griffin RG (2002) 3D TEDOR NMR Experiments for the Simultaneous Measurement of Multiple Carbon−Nitrogen Distances in Uniformly 13C, 15N-Labeled Solids, Journal of the American Chemical Society 124, 10728–10742. [PubMed: 12207528]

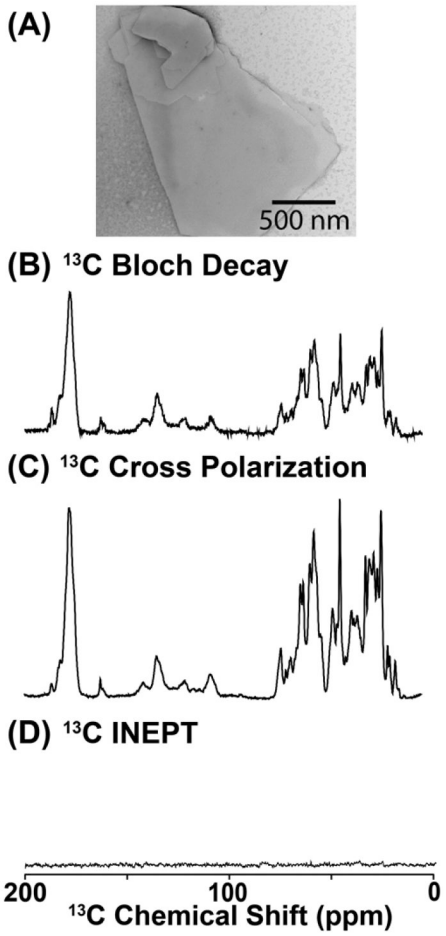

Figure 1.

Characterization of VDAC2 samples with electron microscopy and solid state NMR. (A) Electron micrograph of VDAC2-embedded 2D DMPC lipid crystals. The lower right bar corresponds to a length of 500 nm. (B-D) One-dimensional ^{13}C NMR spectra of human VDAC2 in DMPC lipid 2D crystals measured at 900 MHz field strength and 20 kHz spinning frequency at 283 K: (B) Bloch decay (i.e. direct ^{13}C excitation), (C) cross polarization, and (D) INEPT spectra. The ^{13}C CP spectrum was measured with 256 scans, the Bloch decay spectrum 512 scans, and the INEPT spectrum 1024 scans.

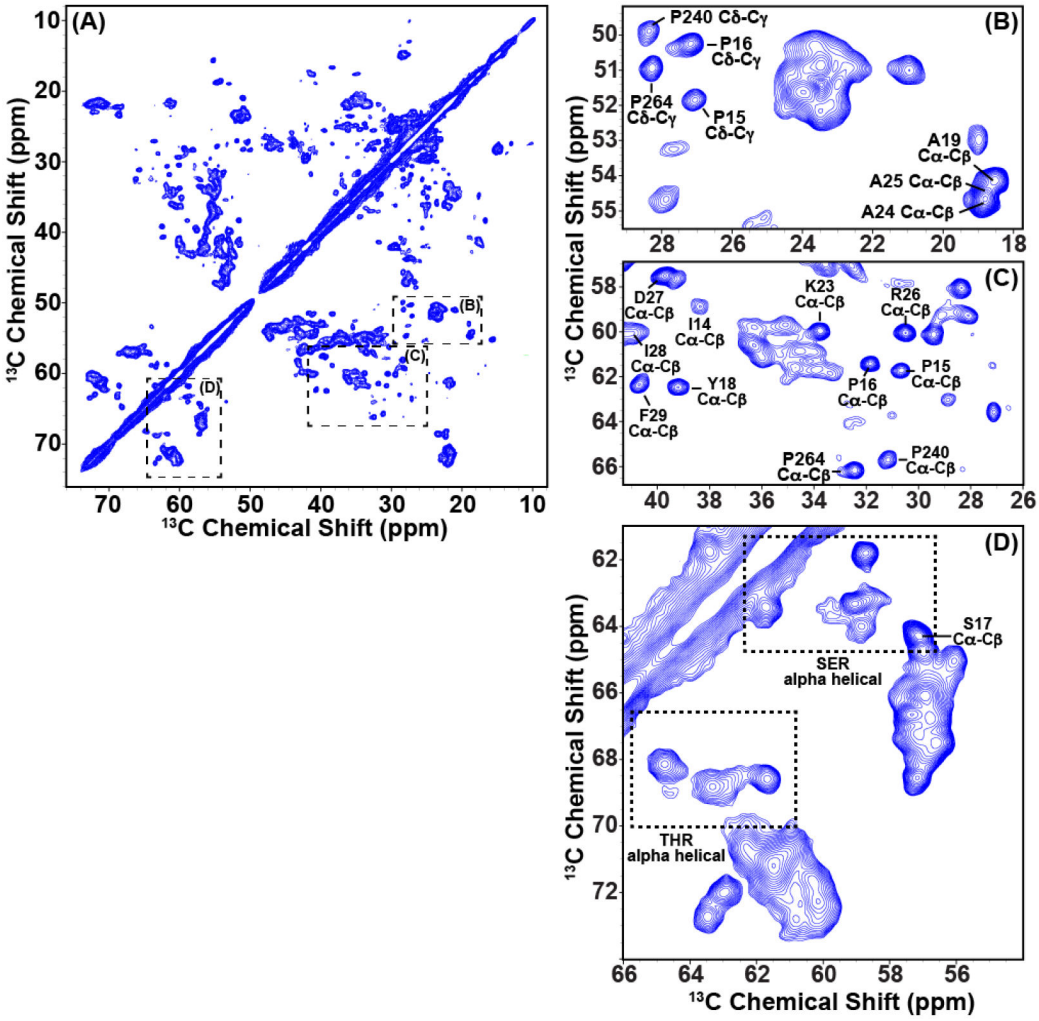

Figure 2.

Representative 2D ^{13}C–^{13}C RFDR correlation spectrum of U-^{13}C, ^{15}N-VDAC2 in DMPC 2D lipid crystals measured at $\omega_{0H}/2\pi$=900 MHz, $\omega_r/2\pi$=20 kHz, T=283 K, with τ_{mix}=1.8 ms RFDR and $\omega_{1H}/2\pi$=83 kHz TPPM decoupling during evolution and acquisition periods. The experiment averaged 48 scans for a total acquisition time of approximately 24 hours. Panel A shows the full aliphatic region of the spectrum, and Panels B and C show selected expansions of the spectrum with annotated resonance assignments. Assignments were obtained via 3D ^{15}N-^{13}C-^{13}C experiments in this case a ZF-TEDOR-RFDR correlation experiment that simultaneously provided intra- and inter-residue connectivities, as described in more detail below.

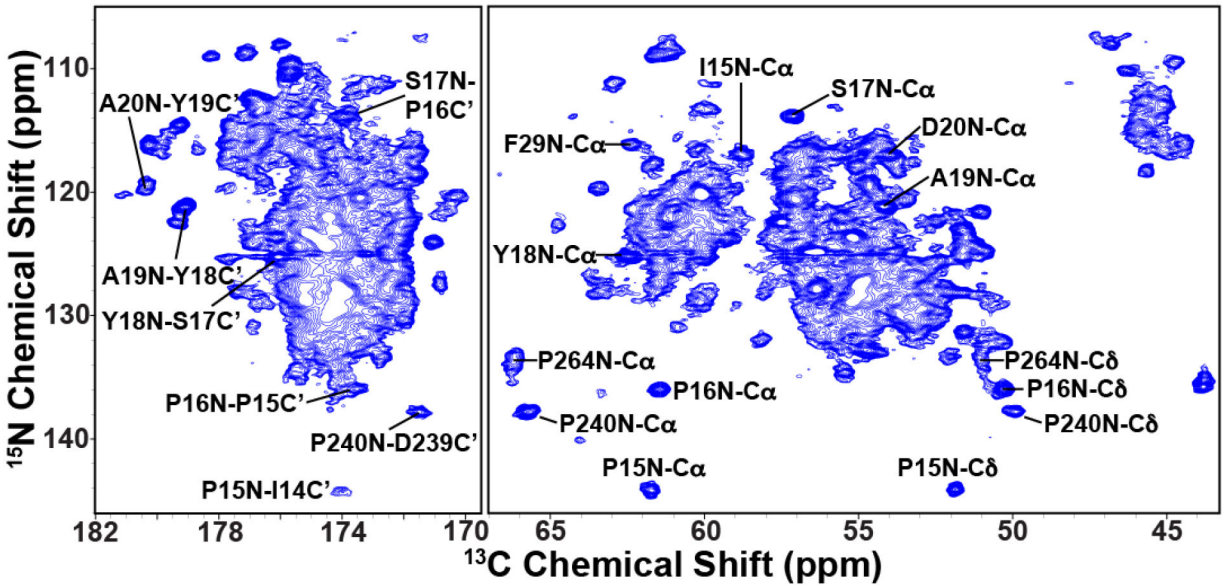

Figure 3.

(A) 2D $^{15}N–^{13}C$ zf-TEDOR correlation spectrum of U-^{13}C, ^{15}N-VDAC2 in DMPC 2D lipid crystals recorded at $\omega_{0H}/2\pi$=900 MHz, $\omega_r/2\pi$=20 kHz, and T=283 K, with τ_{mix}=1.8 ms RFDR and $\omega_{1H}/2\pi$=83 kHz TPPM decoupling. TEDOR mixing was optimized for one-bond transfers. Left and right panels show expanded $^{15}N–^{13}C'$ and $^{15}N–^{13}C\alpha$ regions, respectively. The experiment averaged 128 scans for a total measurement time of approximately 12 h. Assignments for a subset of resolved signals are annotated.

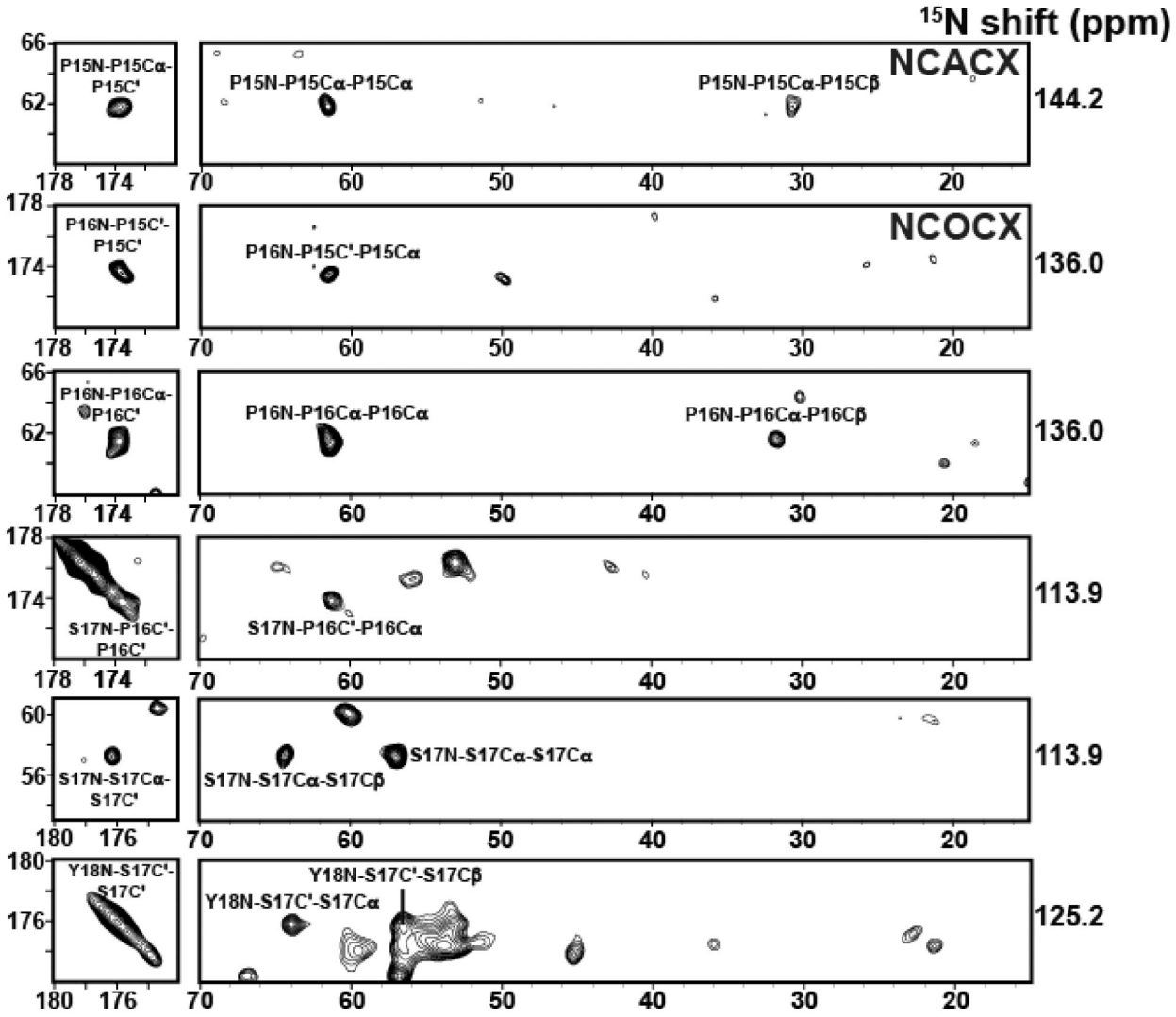

Figure 4.

Sequential assignment of VDAC2 resonances. Representative strip plots from the 3D zf-TEDOR-RFDR correlation experiment showing alternating NCACX and NCOCX regions used to assign residues P15 through Y18. Assigned signals are annotated in each strip plot. The numbers listed to the right of the strip plots indicate the ^{15}N backbone chemical shifts that connect adjacent ^{13}C spin systems.

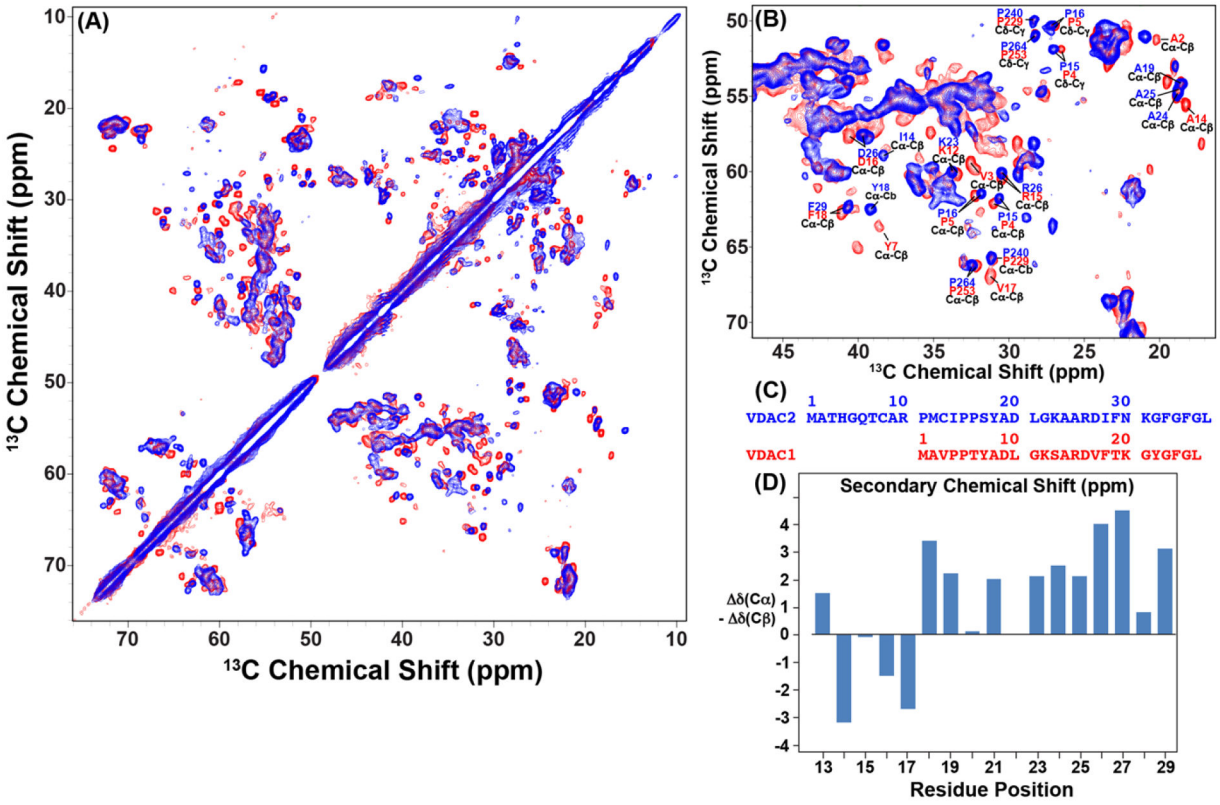

Figure 5.

Comparison of SSNMR ^{13}C–^{13}C correlation spectra of VDAC2 and VDAC1 in DMPC lipid bilayers. (A) Superposition of the aliphatic region of 2D ^{13}C–^{13}C RFDR correlation spectra of U-^{13}C, ^{15}N-VDAC2 (blue) and U-^{13}C, ^{15}N-VDAC1 (red). Both spectra were recorded at $\omega_{0H}/2\pi$=900 MHz, $\omega_r/2\pi$=20 kHz, T=283 K, with τ_{mix}=1.8 ms RFDR and $\omega_{1H}/2\pi$=83 kHz TPPM decoupling during evolution and acquisition periods. Both spectra were processed identically and displayed at the same contour level. (B) Expansion of the aliphatic region, using the same color scheme as in Panel A with assignments for residues from the N-termini. (C) Sequences of VDAC1 and VDAC2 N-termini. (D) Secondary chemical shifts calculated from the VDAC2 assigned residues 13 to 29.

Table 1.

Chemical shifts listed in ppm of assigned VDAC2 resonances.

Amino Acid	N	C'	Cα	Cβ	Cγ	Cδ	
C13			57.1	32.5			
I14		174.1	58.7	38.3	27.5		16.7
P15	144.2	173.7	61.7	30.6	27.0	51.8	
P16	136.0	173.9	61.5	31.8	27.2	50.3	
S17	113.9	176.2	57.2	64.3			
Y18	125.2	179.1	62.5	39.2			
A19	121.2	177.5	54.2	18.5			
D20	117.1		54.0	40.7			
L21			56.4	40.6			
G22							
K23	124.4		60.1	33.8			
A24	127.2		54.8	18.8			
A25	121.0	180.5	54.2	18.7			
R26	120.2			60.1	30.5		
D27				57.5	39.7		
I28			61.1	39.4			
F29	116.4	176.8	62.4	40.7			
D239		171.5	53.8				
P240	138.0	177.5	65.7	31.2	28.3	49.9	
R263		174.2	55.0				
P264	133.8	177.1	66.2	32.4	28.3	51.0	